https://doi.org/10.1016/j.eml.2020.100771

Automated identification and characterization of two-dimensional materials via machine learning-based processing of optical microscope images

Juntan Yang, Haimin Yao*

Department of Mechanical Engineering, The Hong Kong Polytechnic University, Hung Hom, Kowloon, Hong Kong SAR, China

Abstract

Mechanical characterization of two-dimensional (2D) materials has always been a challenging task due to their extremely small thickness. The current prevailing methods to measure the strength of 2D materials normally involve sophisticated testing facilities and complicated procedures of sample preparation, which are usually costly and time-consuming. In this paper, we propose a cost-effective and rapid approach to characterizing the strength of 2D materials by processing optical microscope images of the mechanically exfoliated 2D materials. Specifically, a machine learning-based model is developed to automate the identification of 2D material flakes of different layers from the optical microscope images, followed by the determination of their lateral size. The statistical distribution of the flakes' size is obtained and used to estimate the strength of the associated 2D material based on a distribution-property relationship we developed before. A case study with graphene indicates that the present machine learning-based method, as compared to the previous manual one, enhances the efficiency of characterization by more than one order of magnitude with no sacrifice of the accuracy.

Keywords:

Image processing and recognition; Machine learning; Inverse problem; Mechanical characterization

* Corresponding author.

Email address: mmhyao@polyu.edu.hk (H. Yao)

1. Introduction

Mechanical properties of two-dimensional (2D) materials play important roles in almost every aspect of their applications in various fields [1, 2]. The past decade has witnessed considerable efforts and breakthroughs in the characterization of the mechanical properties of 2D materials [3]. The pioneering and probably the most commonly used method is the indentation on suspended circular 2D material films using atomic force microscopy (AFM) [2, 4-6]. Mechanical properties such as Young's modulus and strength can be determined by regression analysis of the measured force-deflection relationship under indentation with a theoretical prediction [2, 4-6]. Recently, the development of micro-electromechanical systems facilitates more complex manipulations of the 2D material specimen and provides versatile platforms for *in situ* mechanical tests in a scanning electron microscope (SEM)/transmission electron microscope (TEM) [7, 8]. However, these methods normally involve specialized equipment and complicated operating procedure, which are usually costly and time-consuming [9]. The associated micro-mechanical devices are also vulnerable to external loads and adverse experimental conditions [9, 10]. These limitations bring up challenges to the fast and accurate characterization of 2D materials. Nevertheless, our earlier study revealed that the statistical distribution of the lateral size of the mechanically exfoliated 2D material flakes is intrinsically correlated to their mechanical properties specifically fracture strength [11]. This offers us a new approach to deducing the strength of 2D materials from their size distribution. This method is cost-effective and easy to be implemented since the information of size distribution can be easily acquired with an optical microscope (OM) [10]. However, the identification and size measurement of 2D materials from the OM heavily relies on a visual inspection and personal judgment, which largely limits the efficiency of this method [12]. To solve this problem, here we propose to automate this process by using image recognition and processing techniques [12-22], while the implementation of this idea still encounters some practical challenges. First, the low contrast between the 2D materials and the substrate makes the identification and classification of them difficult, especially for the monolayer ones [23]. Meanwhile, the presence of the unavoidable adhesive residue and image noise increases the possibility of misidentification [12]. Moreover, 2D material flakes usually exhibit irregular shapes [1], which further increases the difficulty of automatic identification. Recently, machine learning techniques such as support vector machine (SVM)[12, 24], clustering analysis[13] and convolutional neural networks (CNN)[25-29] have been applied to automate the identification and

classification of materials using their image features. In general, unsupervised techniques like clustering analysis and CNN are more robust, but they require immense training data and higher computing resource. On the other hand, supervised machine learning like SVM deals with prelabeled training data, which not only reduces the computational expense but achieves good accuracy especially when the dimension of the feature vector is low. In view of these features, a supervised machine learning-based classification model is proposed to identify 2D materials of different layers in the light of their color features in an OM image, followed by the size measurement of the identified flakes. The whole recognition process is implemented automatically with custom codes, enabling a rapid acquisition of the statistical distribution of the flake size. In combination with a theoretical model that correlates the size distribution and the strength of the 2D material, characterization of the strength of the associated 2D material can be achieved. In the rest of this paper, elaboration of this procedure will be made by using mechanically exfoliated graphene flakes as an example.

2. Methods

2.1 Pretreatment of optical microscope images

Due to the experimental uncertainties such as non-uniform illumination, decaying of camera sensor over time and so on, the image taken by an optical microscope may not be directly used for identification and characterization. One of the most common problems is the vignetting effect induced by the lens shading [30, 31]. As shown in Fig. 1(a)-(b), the color profile of the pixels of the background varies largely with the location. This would greatly impair the accuracy of the subsequent identification of graphene flakes. To improve the image quality, a series of numerical image enhancement treatments are applied. First, a median filter is applied to the OM image to reduce noise by taking the window size of the filter as 3 pixels [10]. Next, a polynomial function is adopted to fit the color profile of the background [32]. Here, the polynomial is taken as a quadratic function, which is a good compromise between accuracy and efficiency [10]. Finally, the fitting background is subtracted from the original image, resulting in an image with significant improvement in both quality and uniformity, as displayed in Fig. 1(c)-(d). The treated image now is ready for the identification and subsequent characterization of graphene.

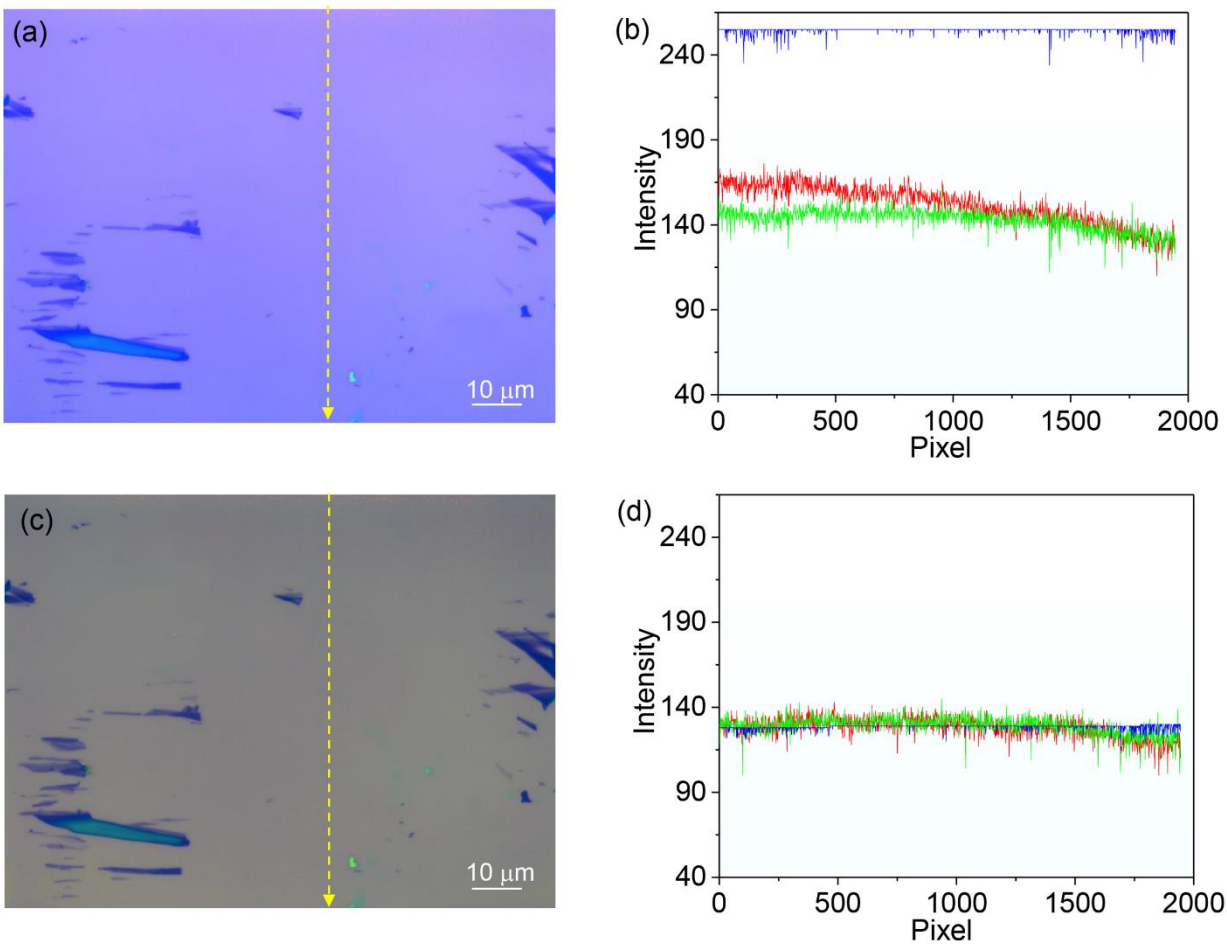

Fig. 1. Pretreatment of an OM image of mechanically exfoliated graphene. (a) A typical OM image of graphene on SiO_2/Si substrate. (b) Color profiles along the path indicated by the yellow dashed line in (a). Curves in red, green and blue represent the intensities of the red, green and blue of the pixels, respectively. (c) OM image of graphene after pretreatment. (d) Color profiles along the same path as indicated in (a) after pretreatment.

2.2 Identification of graphene flakes

To identify graphene flakes from OM images at an affordable computational cost, we use the support vector machine (SVM), a supervised machine learning method, to classify graphene of different layers and substrate according to their color features in the image. Define a feature vector $\boldsymbol{x}=(R, G, B)$, where R, G and B represent the intensities of red, green and blue (RGB) of a pixel, respectively. For an 8-bit color graph as we use, R, G and B take integers from 0 to $(2^8-1)=255$. First, we select a typical OM image as the training image and extract sufficient training data set

$(\boldsymbol{x}_i, y_i) = (R_i, G_i, B_i, y_i)$ from it, where $\boldsymbol{x}_i$ is the feature vector of the *i*-th pixel in the training data set, and y_i labels the substance to which the *i*-th pixel pertains. For example, $y_i = 1$ represents the substrate, $y_i = 2$ represents monolayer graphene, $y_i = 3$ represents bilayer graphene, *etc*. The substance labels (y_i) in the training image are determined manually in the light of the contrast between the few-layer graphene and substrate [33]. Fig. 2(a) shows the training data points of color feature extracted from a training image. For simplicity, here the projection of the data points on the red-green (R-G) plane is shown. We can see that the red and green intensities corresponding to graphene of different layers are distributed in distinct realms on the R-G plane. Data points pertaining to the substrate exhibit the highest red and green intensities. Due to the presence of graphene and the increase of layer numbers, the intensities of both colors decrease. The complex distribution of the data points on the R-G plane makes it difficult to delimitate different realms with linear boundaries. The Gaussian kernel function is adopted to determine the nonlinear boundaries between adjacent realms (see **Supplementary material**). Meanwhile, there are some data points of adjacent realms slightly overlap near the boundaries in Fig. 2(a). These abnormal data points may result from noise or local nonuniformity. The slack variable vector is used to avoid overfitting caused by these data points (see **Supplementary material**) [34, 35]. Finally, a classification model is obtained from the training data (see Fig. 2(b)), which delimits the R-G plane into five distinct realms with each realm enclosing the R-G information corresponding to a certain type of substance such as substrate, monolayer graphene, bilayer graphene and so on. After obtaining the classification model, one can determine the substance label, y_i, for each pixel in a testing image according to its color vector $\boldsymbol{x}_i$. Then, the size of a mechanically exfoliated graphene flake, which is defined as the length along the peeling direction of exfoliation [11], can be determined from the distance between the leftmost and the rightmost pixels of the flake given that the peeling direction is horizontal.

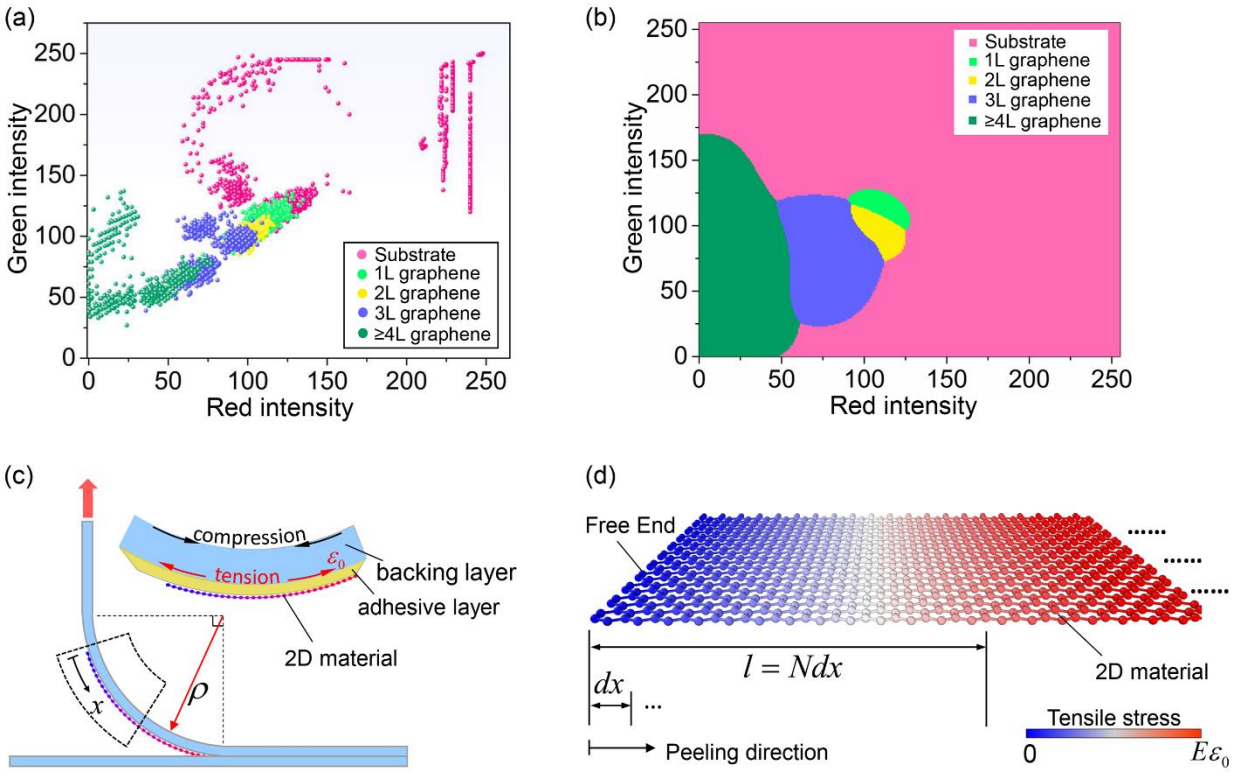

Fig. 2. (a) The data points used to train the classification model. (b) The as-trained classification model on the R-G plane. (c) Schematic of the peeling process during mechanical exfoliation with inset showing the closeup near the detaching point (not in scale). (d) Schematic diagram of the graphene layer under tension for fracture analysis.

2.3 Mechanical property characterization

Our previous study indicated that the size distribution of mechanically exfoliated graphene flakes is not entirely random but follows certain statistical patterns [11, 36]. In fact, the flake size is determined by the fracture behavior of graphene, which is synergistically controlled by the external load and its intrinsic mechanical properties. Considering the brittle nature of graphene, we assume it follows the Weibull strength theory. Therefore, the survival (no fracture) probability of a graphene flake with a size of Δx under stress σ is given by [37]

$$P\left(\Delta x,\sigma\right)=\exp\left(-\frac{\Delta x}{l_0}\left(\frac{\sigma}{\sigma_0}\right)^{\alpha}\right) \tag{1}$$

where α is the Weibull modulus, l_0 is the reference size with σ_0 being the corresponding Weibull characteristic strength. Since the survival probability of material should be independent of the selection of characteristic parameters, $l_0\sigma_0^{\alpha}$ in Eq. (1) should be constant for a given material [38]. Without loss of generality, in this paper, we take l_0 = 1 μm [11]. Due to the bending of the Scotch tape at the peeling edge, the lower side of its backing layer undergoes tensile strain $\varepsilon_0 = t_B\sqrt{\gamma b / 2K}$ (see Fig. 2(c)), where t_B is the thickness of the tape backing layer; γ, b and K are the adhesion energy, width and bending stiffness of the tape respectively. By taking $\gamma = 181\ \mathrm{N\cdot m^{-1}}$ [39], $b = 19$ mm, $t_B = 0.08$mm, and $K = 0.6526\ \mathrm{N\cdot mm^2}$ [11], it is estimated that $\varepsilon_0 = 12.9\%$. Such tension is transferred to the graphene via the adhesive layer, resulting in non-uniform tension of the graphene layer. Consider a graphene part with a size of l as shown in Fig. 2(d). It is composed of N infinitesimal segments each with a size of *dx*. The tensile stress in each segment can be deemed uniform. The probability of attaining a graphene flake with size larger than l equals the probability of survival of N consecutive segments during the exfoliation, i.e. $P\left(\text{size} \geq l\right) = \prod_{i=1}^{N} P\left(dx, \sigma_i\right)$, where σ_i is the stress of the *i*-th segment. The probability of obtaining graphene flakes with a length smaller than l can be thus is given by

$$P\left(\text{size} \leq l\right) = 1 - P\left(\text{size} \geq l\right) = 1 - \prod_{i=1}^{N} P\left(dx, \sigma_i\right) \tag{2}$$

By taking the derivative of Eq.(2) with respect to l, the probability density, which represents the size distribution of mechanically exfoliated graphene flakes, is given by [11]

$$p(l) = \frac{dP\left(\text{size} \leq l\right)}{dl} = l_0^{-1}\eta^{\alpha}\left[1 - \exp\left(-\bar{l}\right)\right]^{\alpha} \exp\left(-\left(\beta l_0\right)^{-1}\eta^{\alpha}\int_0^{\bar{l}}\left[1 - \exp\left(-x\right)\right]^{\alpha} dx\right) \tag{3}$$

where $\bar{l} = l / l_0$, $\eta = E\varepsilon_0 / \sigma_0$, $\beta = \sqrt{G_A / Et_A t}$. Here, E and t represent Young's modulus and thickness of the graphene, respectively; G_A and t_A represent the shear modulus and thickness of the adhesive layer in the tape, respectively. The parameters α, β, η in Eq. (3) can be determined by regression analysis using the size distribution obtained by the machine learning-based method

above. Taking $E = 1$ TPa [2, 5] and $\varepsilon_0 = 12.9\%$, the Weibull characteristic strength σ_0 can be derived from η. The expectation of the strength can be then determined through [40, 41]

$$\langle \sigma_s \rangle = \left(\frac{l}{l_0} \right)^{-\frac{1}{\alpha}} \sigma_0 \Gamma\left(1 + \frac{1}{\alpha}\right) \tag{4}$$

where $\Gamma(\cdot)$ is the Gamma function. Although the above characterization is implemented on graphene, the characterization method can be extended to other 2D materials, provided that they fracture in a brittle manner and the theoretical model is applicable. Moreover, the essence of our method is to apply the correlation between mechanical properties (strength) and the structural feature (flake size) to deduce the associated property. This concept can be further generalized to the characterization of mechanical properties other than strength as long as the correlation can be revealed. It is also worth noting that the above characterization is based on a quasi-static exfoliation process. Higher peeling velocity results in higher tensile stress in the 2D material layer and smaller as-exfoliated flakes. Likewise, reducing the peeling angle below 90° also has a similar effect on the flake size. Consideration of these effects requires more sophisticated mechanics models [42, 43].

3. Results and discussions

Fig. 3(a) shows a typical OM image of mechanically exfoliated graphene with a resolution of 2592×1944 pixels corresponding to actual dimensions of 115 × 86 μm. Fig. 3(b) shows the identification results of the graphene flakes. In line with the theoretical model in which the 2D material is assumed as uniform in thickness, here we only focus on the monolayer graphene flakes which are enclosed by their bounding boxes in Fig. 3(b). The size of these flakes is around a couple of microns.

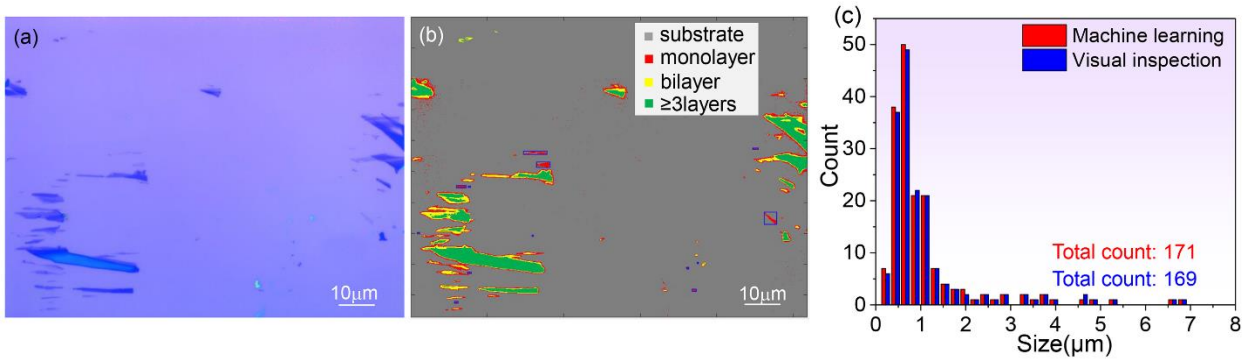

Fig. 3. Results of graphene identification and characterization. (a) A typical OM image for testing; (b) identification results of graphene flakes corresponding to the test image shown in (a), the blue rectangle represents the bounding box of each identified monolayer graphene flake; (c) statistics of size of monolayer graphene flakes obtained from machine learning-based recognition and visual inspection, respectively. The interval of flake size, 0.22 μm.

Automatic identification and size measurement are performed on 18 OM images. 171 monolayer graphene flakes are identified in total. The histogram in Fig. 3(c) shows the statistics of the size of these identified graphene flakes in comparison to that obtained from manual visual inspection. The size of the graphene flakes exhibits an asymmetrical distribution about its mean value. Results obtained by machine learning-based identification show no significant difference from those obtained by visual inspection. A more quantitative comparison shown in Table 1 indicates that the proposed machine learning-based method can achieve comparable recall and precision as the manual inspection does. However, the processing time used in this method is 136 s, which is one order of magnitude less than that spent by the manual method, implying that the efficiency of identification of graphene and size measurement is greatly improved.

Table 1. Comparison of the performance between the proposed machine learning-based method and the manual inspection-based method

	Identified count	Correct count	Actual number	Recall	Precision	Time consumed (second)
Machine learning	171	168	170	98.8%	98.2%	136
Manual inspection	169	169	170	99.4%	100%	~1800

Notes: Identified count refers to the number of monolayer graphene flakes identified; *Correct count* refers to the number of the identified monolayer graphene flakes that are indeed monolayer; *Actual number* refers to the actual number of monolayer graphene flakes existing in the images, which is determined by cross-checking of the machine learning-based and manual inspection methods; *Recall* is the ratio of the *Correct count* to the *Actual number*; *Precision* is the ratio of the *Correct count* to the *Identified count* [44].

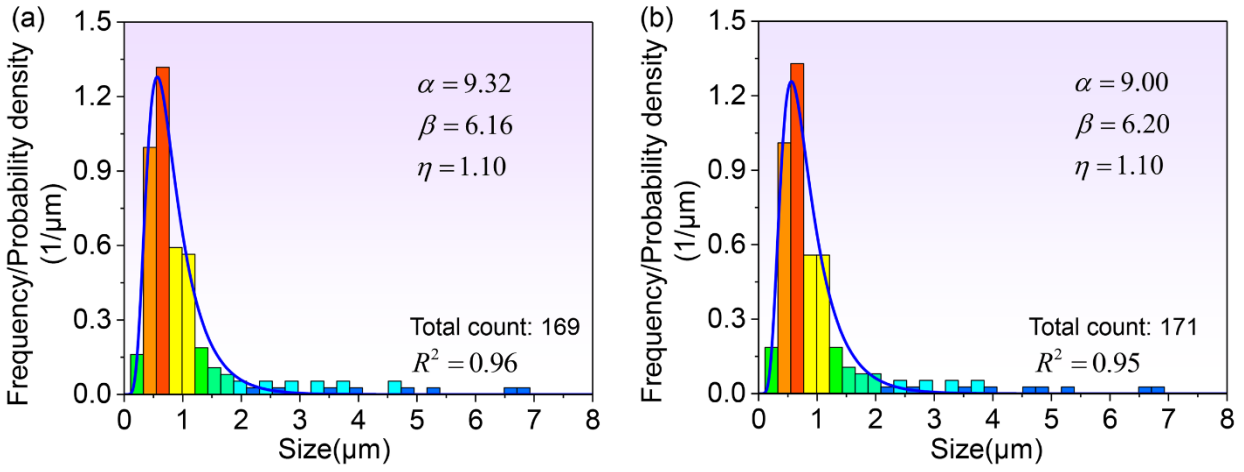

Fig. 4. The size distribution of monolayer graphene flakes obtained by (a) manual visual inspection and (b) machine learning-based automatic characterization method. The frequency density is obtained by dividing the count of each bar shown in Fig 3(c) by the product of total count and the bar width. The blue curves are the regression curves based on the theoretical expression (Eq. (3)).

Based on the statistical distribution shown in Fig. 3(c), the frequency density, which can be deemed as the measured probability density in practice, is calculated and shown in Fig. 4, followed by regression analysis using Eq. (3). The high R^2 (coefficient of determination) in both cases indicates that Eq. (3) describes the probability density of the flake size very well. The values of α and η determined by the regression analysis allow us to derive the characteristic strength σ_0. Thus, the expectation of the strength of graphene, as given by Eq. (4), is plotted in Fig. 5. It can be seen that the results obtained by machine learning-based characterization and visual inspection are quite close, and both in reasonable agreement with the data reported in the literature, as illustrated by the scatter points. However, some data points exhibit a relatively significant deviation from our prediction. For example, the black circle in Fig. 5 indicates that for a graphene monolayer with a size of 3 μm, the strength is about 60 GPa [45], which is far below our prediction. This may be attributed to the edge defects induced by focused ion beam (FIB) in the sample preparation process. These defects would largely affect the strength of the test specimen, as demonstrated by the authors with molecular dynamics simulation [45]. In view of this fact, we can conclude that our characterization results are consistent with those reported in the literature. The validity of the proposed machine learning-based method is confirmed.

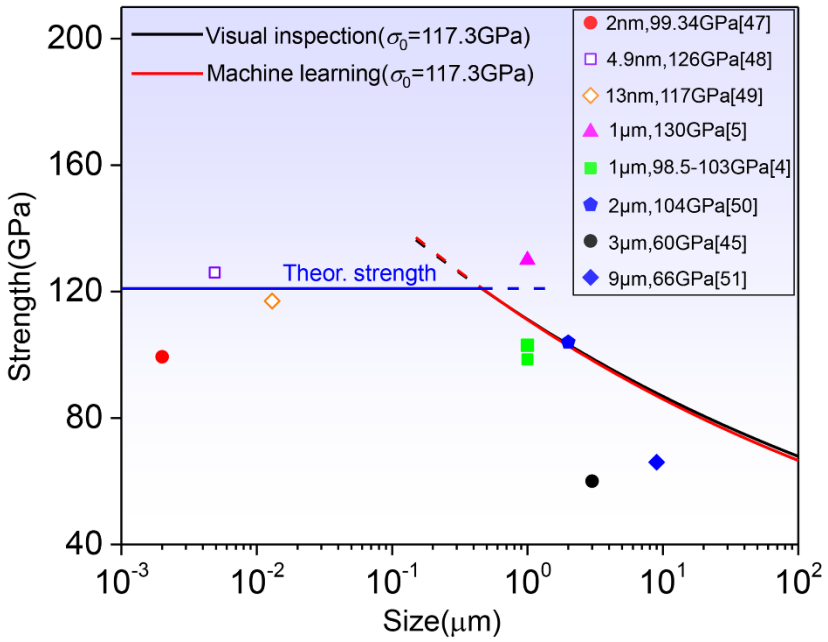

Fig. 5. The expected strength of graphene as a function of flake size obtained using the present machine learning-based method in comparison with that by the prior visual inspection-based method. The strength-size curves are capped by the theoretical strength of graphene (121GPa) obtained from the *ab initio* calculation [46]. The scatter symbols represent the results reported in the literature [45, 47-51]. The hollow symbols pertain to the computational results while the solid symbols represent the experimental results.

4. Conclusion

In summary, we reported an efficient approach to characterizing the thickness, size, and strength of mechanically exfoliated 2D materials. A machine learning-based classification model is developed to identify 2D material flakes with different thicknesses from their optical microscope images, followed by the measurement of the flake size using image processing techniques. This procedure is automated, enabling us to quickly identify a sufficient number of 2D material flakes and obtain the statistical distribution of their size which, in the light of a theoretical model we developed before, can be applied to decipher the strength of the 2D materials. A case study on graphene proved that our automated method could achieve comparable accuracy as the manual visual inspection does in obtaining the size distribution of graphene flakes, while the efficiency is enhanced by more than one order of magnitude. The strength of graphene characterized by our method shows good agreement with those reported in the literature. Our work establishes a new paradigm of incorporating mechanics modeling and machine learning to achieve high-efficiency

material characterization. The method developed in this paper can also be extended to other 2D materials and is believed to provide valuable references to the high-throughput characterization of 2D materials in various fields.

Declaration of competing interest

The authors declare that they have no conflict of interest.

Acknowledgments

This work was supported by the Research Grant Council of Hong Kong (Grant No.: PolyU152064/15E) and the General Research Fund of Hong Kong Polytechnic University (G-YBXP).

Appendix A. Supplementary data

Details on the machine learning technique can be found in the Supplementary material related to this article.

References

1. Yang, J., et al., *Edge orientations of mechanically exfoliated anisotropic two-dimensional materials.* Journal of the Mechanics and Physics of Solids, 2018. **112**: p. 157-168.

2. Akinwande, D., et al., *A review on mechanics and mechanical properties of 2D materials—Graphene and beyond.* Extreme Mechanics Letters, 2017. **13**: p. 42-77.

3. Cao, C., Y. Sun, and T. Filleter, *Characterizing mechanical behavior of atomically thin films: A review.* Journal of Materials Research, 2014. **29**(3): p. 338-347.

4. Lee, G.-H., et al., *High-strength chemical-vapor–deposited graphene and grain boundaries.* Science, 2013. **340**(6136): p. 1073-1076.

5. Lee, C., et al., *Measurement of the elastic properties and intrinsic strength of monolayer graphene.* Science, 2008. **321**(5887): p. 385-388.

6. Bertolazzi, S., J. Brivio, and A. Kis, *Stretching and breaking of ultrathin MoS2.* ACS Nano, 2011. **5**(12): p. 9703-9709.

7. Cao, C., et al., *In situ TEM tensile testing of carbon-linked graphene oxide nanosheets using a MEMS device.* Nanotechnology, 2016. **27**(28): p. 28LT01.

8. Jang, B., et al., *Uniaxial fracture test of freestanding pristine graphene using in situ tensile tester under scanning electron microscope.* Extreme Mechanics Letters, 2017. **14**: p. 10-15.

9. Wang, Y., et al., *3D printed micro-mechanical device (MMD) for in situ tensile testing of micro/nanowires.* Extreme Mechanics Letters, 2019. **33**: p. 100575.

10. Dickinson, W.W., et al., *High-throughput optical thickness and size characterization of 2D materials.* Nanoscale, 2018. **10**(30): p. 14441-14447.

11. Yang, J., et al., *Deciphering mechanical properties of 2D materials from the size distribution of exfoliated fragments.* Extreme Mechanics Letters, 2019: p. 100473.

12. Lin, X., et al., *Intelligent identification of two-dimensional nanostructures by machine-learning optical microscopy.* Nano Research, 2018. **11**(12): p. 6316-6324.

13. Masubuchi, S. and T. Machida, *Classifying optical microscope images of exfoliated graphene flakes by data-driven machine learning.* npj 2D Materials and Applications, 2019. **3**(1): p. 4.

14. Bishop, C.M., *Pattern recognition and machine learning*. 2006: springer.

15. LeCun, Y., Y. Bengio, and G. Hinton, *Deep learning.* Nature, 2015. **521**(7553): p. 436.

16. Shen, D., G. Wu, and H.-I. Suk, *Deep learning in medical image analysis.* Annual review of biomedical engineering, 2017. **19**: p. 221-248.

17. Litjens, G., et al., *A survey on deep learning in medical image analysis.* Medical image analysis, 2017. **42**: p. 60-88.

18. Menden, M.P., et al., *Machine learning prediction of cancer cell sensitivity to drugs based on genomic and chemical properties.* PLoS One, 2013. **8**(4): p. e61318.

19. Ball, N.M. and R.J. Brunner, *Data mining and machine learning in astronomy.* International Journal of Modern Physics D, 2010. **19**(07): p. 1049-1106.

20. Ivezić, Ž., et al., *Statistics, data mining, and machine learning in astronomy: a practical Python guide for the analysis of survey data*. Vol. 1. 2014: Princeton University Press.

21. Chen, C., et al. *Deepdriving: Learning affordance for direct perception in autonomous driving*. in *Proceedings of the IEEE International Conference on Computer Vision*. 2015.

22. Maqueda, A.I., et al. *Event-based vision meets deep learning on steering prediction for self-driving cars*. in *Proceedings of the IEEE Conference on Computer Vision and Pattern Recognition*. 2018.

23. Blake, P., et al., *Making graphene visible.* Applied Physics Letters, 2007. **91**(6): p. 063124.

24. Cubuk, E.D., et al., *Identifying structural flow defects in disordered solids using machine-learning methods.* Physical Review Letters, 2015. **114**(10): p. 108001.

25. Masubuchi, S., et al., *Autonomous robotic searching and assembly of two-dimensional crystals to build van der Waals superlattices.* Nature Communications, 2018. **9**(1): p. 1-12.

26. Masubuchi, S., et al., *Deep-learning-based image segmentation integrated with optical microscopy for automatically searching for two-dimensional materials.* npj 2D Materials and Applications, 2020. **4**(1): p. 1-9.

27. Han, B., et al., *Deep Learning Enabled Fast Optical Characterization of Two-Dimensional Materials.* arXiv preprint arXiv:1906.11220, 2019.

28. Saito, Y., et al., *Deep-learning-based quality filtering of mechanically exfoliated 2D crystals.* npj Computational Materials, 2019. **5**(1): p. 1-6.

29. Onodera, M., et al., *Assembly of van der Waals heterostructures: exfoliation, searching, and stacking of 2D materials.* Japanese Journal of Applied Physics, 2020. **59**(1): p. 010101.

30. Leong, F.W., M. Brady, and J.O.D. McGee, *Correction of uneven illumination (vignetting) in digital microscopy images.* Journal of Clinical Pathology, 2003. **56**(8): p. 619-621.

31. Kim, S.J. and M. Pollefeys, *Robust radiometric calibration and vignetting correction.* IEEE transactions on pattern analysis and machine intelligence, 2008. **30**(4): p. 562-576.

32. Schneider, C.A., W.S. Rasband, and K.W. Eliceiri, *NIH Image to ImageJ: 25 years of image analysis.* Nature Methods, 2012. **9**(7): p. 671.

33. Li, H., et al., *Rapid and reliable thickness identification of two-dimensional nanosheets using optical microscopy.* ACS Nano, 2013. **7**(11): p. 10344-10353.

34. Wu, Q. and D.-X. Zhou, *SVM soft margin classifiers: linear programming versus quadratic programming.* Neural Computation, 2005. **17**(5): p. 1160-1187.

35. Cristianini, N. and J. Shawe-Taylor, *An introduction to support vector machines and other kernel-based learning methods*. 2000: Cambridge university press.

36. Kouroupis-Agalou, K., et al., *Fragmentation and exfoliation of 2-dimensional materials: a statistical approach.* Nanoscale, 2014. **6**(11): p. 5926-5933.

37. Weibull, W., *A statistical distribution function of wide applicability.* Journal of Applied Mechanics, 1951. **103**(730): p. 293-297.

38. Bazant, Z.P. and J.-L. Le, *Probabilistic Mechanics of Quasibrittle Structures: Strength, Lifetime, and Size Effect*. 2017: Cambridge University Press.

39. Pesika, N.S., et al., *Peel-zone model of tape peeling based on the gecko adhesive system.* The Journal of Adhesion, 2007. **83**(4): p. 383-401.

40. Bazant, Z.P. and E.-P. Chen, *Scaling of structural failure.* Applied Mechanics Reviews, 1997. **50**(10): p. 593-627.

41. Klein, C.A., *Characteristic strength, Weibull modulus, and failure probability of fused silica glass.* Optical Engineering, 2009. **48**(11): p. 113401.

42. Zhou, M., et al., *The extended peel zone model: effect of peeling velocity.* The Journal of Adhesion, 2011. **87**(11): p. 1045-1058.

43. Kendall, K., *Peel adhesion of solid films-the surface and bulk effects.* The Journal of Adhesion, 1973. **5**(3): p. 179-202.

44. Tsoumakas, G. and I. Katakis, *Multi-label classification: An overview.* International Journal of Data Warehousing and Mining (IJDWM), 2007. **3**(3): p. 1-13.

45. Cao, K., et al., *Elastic straining of free-standing monolayer graphene.* Nature Communications, 2020. **11**(1): p. 1-7.

46. Liu, F., P. Ming, and J. Li, *Ab initio calculation of ideal strength and phonon instability of graphene under tension.* Physical Review B, 2007. **76**(6): p. 064120.

47. Mazilova, T., E. Sadanov, and I. Mikhailovskij, *Tensile strength of graphene nanoribbons: An experimental approach.* Materials Letters, 2019. **242**: p. 17-19.

48. Wang, M., et al., *Effect of defects on fracture strength of graphene sheets.* Computational Materials Science, 2012. **54**: p. 236-239.

49. Georgantzinos, S., et al., *Size-dependent non-linear mechanical properties of graphene nanoribbons.* Computational Materials Science, 2011. **50**(7): p. 2057-2062.

50. Zandiatashbar, A., et al., *Effect of defects on the intrinsic strength and stiffness of graphene.* Nature Communications, 2014. **5**(1): p. 1-9.

51. Suk, J.W., et al., *Fracture of polycrystalline graphene membranes by in situ nanoindentation in a scanning electron microscope.* physica status solidi –Rapid Research Letters, 2015. **9**(10): p. 564-569.